

A versatile electron-ion coincidence spectrometer for photoelectron momentum imaging and threshold spectroscopy on mass selected ions using synchrotron radiation

Gustavo A. Garcia,^{a)} Héloïse Soldi-Lose, and Laurent Nahon^{b)}

Synchrotron SOLEIL, L'Orme des Merisiers, St Aubin, B.P. 48, 91192 Gif sur Yvette, France

(Received 17 December 2008; accepted 17 January 2009; published online 13 February 2009)

We present a photoelectron-photoion coincidence (PEPICO) spectrometer named DELICIOUS II which combines a velocity map imaging apparatus with a Wiley–McLaren time of flight analyzer for the study of gas phase samples in interaction with the synchrotron radiation (SR). This versatile system is capable of providing photoelectron images on mass-selected compounds with kinetic energy resolutions of $\Delta E/E=5\%$ and a 17 eV bandwidth, as well as threshold photoelectron spectra with a measured resolution of 0.8 meV, as demonstrated on the $3p^{-1}$ ionization of argon. This instrument is also employed for threshold PEPICO experiments, allowing the selection of the parent ion's internal state with sub-meV resolution for light masses (<40 amu) and with typically 2 meV resolution for a mass of 100 amu and with a mass resolving power above 200. The continuous operation of the extraction fields and the independence from the electron's time of flight are well adapted to the quasicontinuous multibunch mode of the SR. This, together with the high transmission of both the electron and ion detection, allows a high coincidence counting rate and facilitates the subtraction of false coincidences. We illustrate the spectrometer's coincidence principle of operation with examples from the valence photoionization of an Ar+Xe mixture and of CF₄. © 2009 American Institute of Physics. [DOI: 10.1063/1.3079331]

I. INTRODUCTION AND EXPRESSION OF THE NEEDS

Gas phase photoionization is a basic photon-matter process widely encountered in nature (interstellar medium, planetary ionosphere), whose study in the laboratory by photoelectron spectroscopy (PES) has made considerable progresses with the availability during the past decades of intense short wavelength light sources such as vacuum ultraviolet (vuv) lasers and synchrotron radiation (SR).¹ PES can either be performed at fixed photon energies with a dispersive analyzer [electrostatic or by time of flight (TOF)], or when a tunable light source is employed, by collecting threshold electrons [also referred to as zero electron kinetic energy (ZEKE)] as a function of the ionizing photon energy. The latter directly provides, by energy conservation, the spectroscopy of the cation electronic structure, and defines the principle of threshold photoelectron spectroscopy (TPES). TPES has a usually very high collection efficiency and a potentially high resolution but lacks any angular resolution and is not adapted to the study of resonant features such as the decay of autoionizing states. Therefore the use of conventional PES versus TPES depends on the scientific needs.

Because of energy (and momentum) conservation, single photoionization of atoms can be fully characterized by PES alone. The molecular case is more complex, since in addition to the internal degrees of freedom in which the energy of the

incoming photon can be stored, such as electronic and/or rovibrational excitation of the resulting ion, part of the energy can also be transferred into translational energy of the cation fragments produced in photodissociation events. In order to fully characterize the energy (and momentum) sharing between the electron and the different ionic fragments, several photoelectron/photoion coincidence (PEPICO) schemes have been developed taking simultaneous advantage of PES, ion momentum, and/or mass spectrometry (MS), sometimes involving the detection of several electron and/or several ions in the case of multiple ionization and core ionization (nPEMICO).²

In the case of valence-shell vuv photoionization, on which we are focusing as from now, dissociative ionization has been studied in terms of spectroscopy, energetics, and thermochemistry via threshold photoelectron photoion coincidence (TPEPICO) experiments, providing dissociation limits and appearance energies, kinetic energy releases (KERs) from state-selected ion, heats of formation, fragmentation breakdown diagrams of state-selected parent ions,^{3–5} as well as ionization energies of radicals.⁶ Note that the TPEPICO method can also be used in the context of bimolecular state-selected ion-neutral reactivity.⁷ Dissociative ionization has also been studied in terms of molecular photoionization and fragmentation dynamics by the study of angle-resolved momentum electron/ion correlations.⁸

On the other hand, imaging techniques, initially introduced by the laser community,⁹ in which the original three-dimensional (3D) electron or ion velocity distribution is projected onto a two-dimensional (2D) position sensitive

^{a)} Author to whom correspondence should be addressed. Electronic mail: gustavo.garcia@synchrotron-soleil.fr.

^{b)} Electronic mail: laurent.nahon@synchrotron-soleil.fr.

detector (PSD) allowing a multiplex and simultaneous measurement of both the radial and angular distributions, have become a widely used and powerful tool in the general field of molecular dynamics.¹⁰ This has been especially the case since the introduction of the velocity map imaging (VMI) concept by Eppink and Parker¹¹ in which the presence of inhomogeneous electric fields producing a lensing effect gives rise to a spectacular deblurring of the images and hence to a considerable improvement in energy resolution. Note that the VMI technique, by its ability to provide crisp images quite regardless of the size of the source volume, is especially well suited for SR-based studies often associated with large source volumes, so that several of these instruments, either used for electron or ion imaging, are being used throughout SR centers.^{12–14}

The combination of these imaging techniques with electron/ion coincidence schemes appears therefore as a powerful tool for the study of molecular photoionization,¹⁵ and it has been applied, for instance, to the study of vectorial correlations in dissociative ionization.^{16,17}

In this paper, we wish to present a versatile and universal electron/ion coincidence imaging spectrometer, called DELICIOUS II, able to perform both TPEPICO and angle-resolved PEPICO (AR-PEPICO). Such a spectrometer has been conceived to be inserted into the SAPHIRS molecular beam (MB) chamber, a permanent end station of the DESIRS vuv beamline¹⁸ of the French third generation synchrotron center SOLEIL. DESIRS is an undulator-based beamline covering the 5–40 eV range with variable polarization and a very high spectral resolution. Its scientific case is manifold including the study of unimolecular reactions such as molecular cation fragmentation as well the dynamics of photoionization of atomic and molecular samples.

The need for versatility of DELICIOUS II is twofold: first, by having a single apparatus to perform most of the scientific case with the SAPHIRS chamber, one saves the time invested in the switching, aligning, and testing of different setups in between two users' beam time; second, it allows to perform, on the very same sample, different and complementary types of spectroscopy (for instance, TPES followed by AR-PEPICO).

In practice, DELICIOUS II is aimed at replacing the former TPEPICO spectrometer¹⁹ of SAPHIRS in which the selection of threshold electrons was done by both a steradiancy aperture as well as by the measurement of electron TOF with respect to the SR light pulse. The drawback of such an approach is the limited resolution (due to uncertainty in the TOF measurement) in the 5–10 meV range, and the need for the "time-structure" operation of the SR ring, a mode of operation which is not very often scheduled on third generation storage rings, and which suffers from a severe flux reduction with respect to the multibunch mode, typically a factor of 5–10, because of the limited electron current that can be stored in a single or in a few electron bunches.

DELICIOUS II will also be an upgrade of DELICIOUS, a SR-optimized VMI spectrometer,¹³ in the sense that DELICIOUS II allows the operation of a VMI on electron (ion) coincidences with ions (electrons). Note that a VMI (ion) has already been implemented in coincidence with electrons (not

analyzed),^{14,20,21} and that photoelectron velocity mapped images have also been recorded previously in coincidence with VMI ions,¹⁷ although the obtained ion mass resolution is not sufficient to fulfill the beamline's scientific case.

DELICIOUS II consists of combining, in a tandem geometry, an electron (or ion) VMI (DELICIOUS) with a Wiley–McLaren TOF (WM-TOF) spectrometer.²² Its specifications are the following:

- (a) Operate in a fully continuous (cw) operation, i.e., with an optimal duty cycle matching the natural SR operation in the multibunch mode as well as with the cw MB of SAPHIRS. In particular, avoid any pulsed electric field for both noise issues on the detector and to avoid the cumbersome subtraction of random coincidences.²³
- (b) Keep all the performances in both the electron and the ion modes achieved by the VMI DELICIOUS alone: ion imaging that we mostly use as a very fine probe of the nozzle-to-skimmer 3D positioning;²⁴ electron imaging with an optimized resolving power of 6% (Ref. 13) and with a 4π collection efficiency up to 17 eV that has been mainly applied, so far, to the study of photoelectron circular dichroism on pure enantiomers of gas phase chiral molecules.^{24,25}
- (c) Perform TPES with the highest possible spectral resolution, at least sub-meV, taking advantage of the broad and easy tunability of SR and of the very high spectral resolution achieved by the DESIRS beamline, providing on a large spectral range the spectroscopy of the ion states with rovibrational resolution.
- (d) Perform TPEPICO by collecting and mass analyzing the coincident ion (the so-called mass analyzed threshold ion) in order, on one hand, to study the fragmentation of energy-selected cations and derive the thermochemical associated data (appearance energy, heats of formation, etc.) and, on the other hand, to be able to perform TPES on mass selected parent ions. This is extremely useful when one deals with a nonpure MB, which is commonly the case of radicals produced by pyrolysis²⁶ or photolysis,²⁷ leading sometimes to a mixture of the radical to be studied and of its precursor.
- (e) Perform AR-PEPICO with high resolution on the electron side (5% in relative kinetic energy) and a mass resolution above 100 (i.e., $\Delta M/M > 100$), and with a high counting rate (typically above 10 000 events/sec) in order to acquire high quality images and to take advantage of the high flux of the beamline. This would allow, for instance, to perform AR-PES on mass selected clusters, and also it would strongly enhance, even in the case of monomers, the performances of the VMI in electron mode by suppressing any unwanted contribution to the electron image. By a simple filtering with the coincident ion peak in the mass spectrum, one could remove any electron contribution from scattered light, background gas, carrier gas of the jet, nonpure jet of radicals, etc. Note that by considering all the electrons regardless of their momentum, one simply gets the mass spectrum of the molecules present in the jet, which is a very fine probe of contamination or thermal

decomposition in the case of a heated sample. Note also that coincidence spectrometers based on the direct full 3D measurement of electron and ion momenta by a dual imaging and TOF technique^{28,29} are capable of covering a broader scientific program than the present AR-PEPICO apparatus (in particular, they can extract molecular frame photoelectron angular distributions) but would not fulfill our requirements because of their limited electron energy resolution,³⁰ especially for fast electrons, and/or their need for a pulsed light source: SR in the time-structure mode or pulsed laser.

- (f) Perform mass-resolved ion imaging for the study of cluster fragmentation, for example, by operating the VMI in the ion mode and using the coincident electron (detected on the TOF side) as a start for the MS analysis.

In Sec. II, we will describe the DELICIOUS II spectrometer and its environment (SAPHIRS MB chamber, SR beamline DESIRS). Then the TPES mode of operation, followed by one of the WM-TOF, will be presented from the conception to the performances. In Sec. V, the coincidence modes PEPICO and TPEPICO will be exposed, illustrated, and discussed. Future prospects will be given in Sec. VI.

II. EXPERIMENTAL SETUP

A VMI spectrometer reconstructs the original Newton's sphere without the need of the time coordinate.³¹ While this is advantageous for continuous light sources, one of the inconveniences is that the reconstruction must be performed *a posteriori*, since the method needs a complete image to work. Thus, contrary to an imaging spectrometer,⁹ one cannot determine the particles' velocity vector by examining a single impact on the detector.

The above statement removes some of the interests of building a coincidence setup where two VMI are coupled together, since only coincidences with particles corresponding to the largest radius would be possible.¹⁷ A more suitable and versatile alternative is to couple a VMI with a spectrometer capable of resolving a single event so that a filtering of the events on an image can be done prior to its inversion. One of the simplest options fulfilling our scientific interests is a WM-TOF spectrometer.²²

A 2D schematic of the apparatus presented in this article is shown in Fig. 1. The VMI part has already been described in detail in a previous article,¹³ the only difference being the aperture plus grid on the repeller plate to sweep the ions through. The WM-TOF consists of two acceleration regions to obtain the space focusing condition for any voltage applied on the extraction plates. The WM-TOF energy focusing condition depends solely on the turn-around time of the ions, which is inversely proportional to the magnitude of the extraction field. Therefore, for TPEPICO experiments involving high (and closely spaced) fragment masses, a compromise must be reached between mass resolution and fast electron discrimination, as we will see in Sec. III.

The combination of imaging techniques with coincidence schemes imposes severe constraints into the type of PSD to be used, since each single event should be recorded

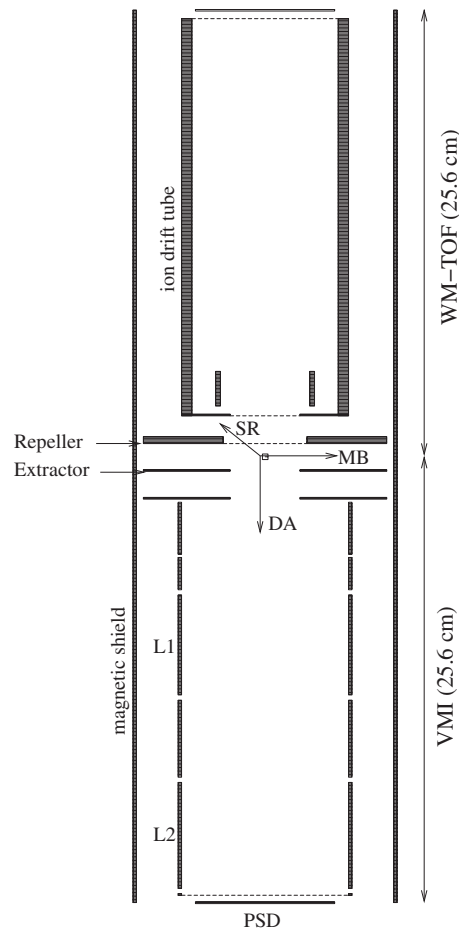


FIG. 1. 2D schematic of the DELICIOUS II spectrometer showing the modified VMI as described in Ref. 13 with its two lenses, L1 and L2, coupled to the two-stage WM-TOF spectrometer. The MB, detector axis, and SR directions are indicated in the figure.

and read one by one. In our case, where the ion TOF can be as low as a few microseconds depending on the extraction voltages, the electron detector should be able to record events at a frequency superior to 100 kHz in order to take advantage of the possible high counting rates reachable with a high flux beamline. This prevents the use of low-repetition rate reading detector, such as the widely used charge coupled device-based camera detector, which would limit the acquisition rate to a few tens of hertz routinely, and, in the best case, to 1 kHz. The PSD mounted on the present VMI has been the subject of a publication.³² Briefly, it is based on a delay-line anode capable of obtaining absolute spatial resolutions better than 50 μm over the 40 mm diameter of the microchannel plates (MCPs) with a dead time below 160 ns (6.25 MHz).

The electron/ion coincidence electronic scheme is shown in Fig. 2. The much faster electron arrives a few tens of nanoseconds after being produced and triggers the internal clock of a CTNM4 multistop time to digital converter (TDC) designed at the Institut de Physique Nucléaire (Orsay, France). The electron arrival also opens a hardware window during which further starts are inhibited. All the stops, four for the electron position and one for the ion TOF, are recorded with a time resolution of 250 ps. The inhibition window width is chosen according to the maximum expected ion

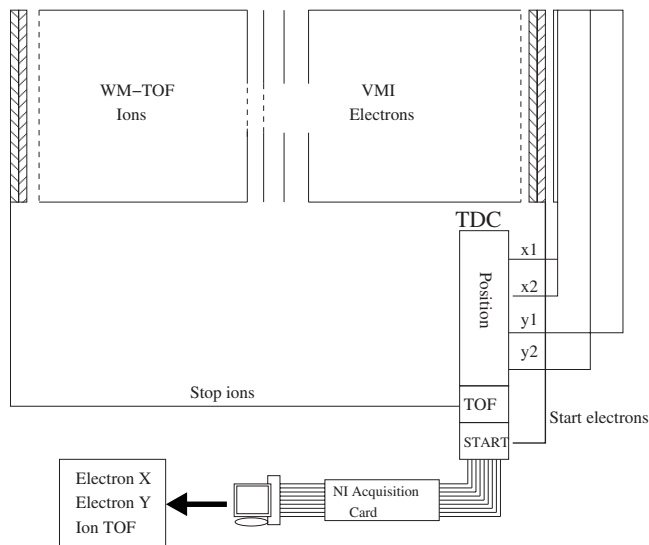


FIG. 2. Data acquisition diagram for the coincidence setup. The preamplified electron signal from the back of the μ channel plates acts as the start. The multistop CTNM4 TDC records the arrival of the four delay anode signals plus the ion TOF with 250 ps resolution.

TOF, typically in the 4–64 μ s. After the window closes, the TDC will accept another start and the process will be repeated. The TDC is interfaced to a personal computer which examines the raw data to generate the electron detector coordinates from the delay anode time signals, and the ion TOF from the WM-TOF detector, for each coincidence event.

There exists also the possibility of performing mass-selected ion imaging where the extraction directions of the electrons and ions are exchanged, much as has been already done by Rolles *et al.*²⁰ In this case, both the ion TOF and ion position come from the VMI while the WM-TOF only gives the start signal to the TDC. However this mode would be detrimental to the mass resolution since the space focusing is lost. Higher mass resolutions have been achieved in ion velocity mapping albeit at the expense of a complicated setup involving the addition of a reflectron.³³

The DELICIOUS II spectrometer is magnetically shielded by two layers of μ -metal and installed vertically inside the SAPHIRS MB chamber.³⁴ As compared to the original design, this chamber has been recently upgraded with a new frame allowing a precise positioning of the chamber's geometrical center with respect to the photon axis. In addition a new motor-controlled XYZ translation stage has been implemented so that a very accurate tuning of the nozzle position with respect to the skimmer can be achieved. Such a critical adjustment is performed in the ion imaging mode²⁴ to optimize the cold-to-thermal contribution in the jet and ensure an optimum transverse alignment of the nozzle with respect to the skimmer and to the VMI main axis.

The photon source is provided by the vuv synchrotron beamline called DESIRS,¹⁸ located at the French synchrotron facility SOLEIL. This undulator³⁵ based beamline provides easy tunability and variable polarization of the photons in the 5–40 eV range. With a high photon flux on the sample in the 10^{12} ph/s range for a 0.1% bandwidth and a measured resolving power of up to 2.5×10^5 at 13 eV and 1.2×10^5 at 21 eV, owing to a 6.65 m normal incidence monochromator,³⁶

the beamline is ideally suited for TPES and TPEPICO/PEPICO studies. This includes AR-PES and AR-PEPICO studies which can benefit from the quick and easy change in polarization (for instance, from linear vertical to horizontal, or to circular) avoiding the need for a cumbersome rotation of the spectrometer around the photon axis. Furthermore, DESIRS offers a high spectral purity due to the upstream presence of a windowless gas filter, which attenuates undulator high harmonics photons, that can be transmitted by the grating's higher order by a factor of up to 200 000.³⁷ The latter is of paramount importance for photoionization studies occurring at relatively low energies, since higher order photons would produce a fast electron background on the images plus spurious ion fragmentation that would strongly impair the reliability of the data.

The skimmed MB is crossed with the photon beam at right angles defining the ionization volume in the center of the VMI installed in the ionization chamber. The distance between the skimmer and the VMI axis is 5 cm. We estimate the MB length at this level to be in the 3–5 mm range depending on the skimmer used, defining the ionization source dimension along the SR axis. Because of the low emittance of SOLEIL, the SR beam transverse dimensions at the focal point are quite small, typically $300 \mu\text{m}$ (horizontal) \times $100 \mu\text{m}$ (vertical). These values set the transverse size of the ionization source volume. Note that if very high flux is needed for the study of extremely diluted targets, we would open the monochromator exit slit by up to $300 \mu\text{m}$, in which case the slit aperture dominates and gives the vertical size of the focal point (up to $300 \mu\text{m}$).

III. TPES MODE OF OPERATION

Despite the large variety of applications of classical PES, limitations of this technique appear when high electron resolution is required, since in general typical resolutions associated with PES lie in the 10 meV range, sometimes down to a few meV. Furthermore, the collection efficiency of electrons with electrostatic analyzers is often poor in PES, which may lead to difficulties in obtaining spectra with acceptable signal-to-noise ratios, as well as preclude efficient experiments performed in coincidence with the corresponding ions because of the high level of false coincidences. To overcome these problems, the TPES approach was introduced a few decades ago, especially for valence-shell single ionization studies. TPES consists of the selection and detection of only electrons having kinetic energies close to zero, the spectroscopy of the ion state being obtained by scanning the photon energy.

In this context, different experimental approaches have been developed, the most commonly employed for SR studies being the TPE detection based on TOF discrimination,^{19,38} the penetrating field,³⁹ and pulsed-field ionization (PFI).⁴⁰ These methods have enabled to achieve resolutions of 5,³⁴ 3,⁴¹ and 0.6 (Ref. 4) meV, respectively. Note that by combining the PFI and the TOF discrimination, Jarvis *et al.*⁴² obtained a TPES resolution down to 0.25 meV on Ar. Improvement of these methods is still possible, since in theory, detection of TPES can be performed with a spec-

tral resolution limited only by the bandwidth of the ionization radiation. Nevertheless, detection based on TOF requires light pulses separated with large time intervals, considerably reducing its application in third-generation synchrotron sources, mostly operating in multibunch mode. PFI-TPES in its most refined mode—coupled with ion detection for TPEPICO (Ref. 4)—requires the use of either the few bunch modes or a hybrid mode with a long dark period, which is not available on many SR centers and is performed to the detriment of mass resolution and with an increased complexity.

In 2003, Sztaray and Baer⁵ introduced an original concept of TPE selection in which velocity focusing optics are used to suppress hot electrons. More precisely, the detector mounted on their spectrometer employed two discrete anodes: a central one to collect the slowest electrons arriving in the middle of the detector, together with a background of fast electrons, and an outer ring to collect only the fast electrons. The TPE contribution is then derived by a subtraction/renormalization of one signal versus the other. This method has the great advantage of operating in a fully continuous mode, well adapted to cw light sources and for which coincidence (TPEPICO) treatment is straightforward.

The TPE selection principle introduced in the present paper represents a major improvement upon the setup of Sztaray and Baer.⁵ It consists of replacing the central and ring anodes by a PSD providing the full imaging capabilities associated with VMI techniques.¹¹ Due to the electrostatic lens created in the VMI extraction region, photoelectrons produced during the ionization process impact the PSD at positions which vary according only to their velocities. Slow electrons are focused on the center of the image whereas faster electrons are spread onto a much larger area around the central spot. The maximum radius R of the impact pattern of photoelectrons with a kinetic energy E is related to the voltage applied on the repeller electrode V_{rep} according to

$$R = C \sqrt{\frac{E}{|q|V_{\text{rep}}}}, \quad (1)$$

where C is a coefficient dependant on the geometry of the VMI and q is the electron's charge.^{11,13} This relation shows that photoelectrons are more spread when a low repeller voltage is applied. Consequently, to discriminate fast electrons from ZEKE, and thus increase the energy resolution, the setup should be operated with the lowest possible repeller voltage. In practice, however, the smallest repeller value will be limited by stray magnetic and electric fields and possible electrostatic aberrations, as shown further down in this section.

Threshold electrons are obtained with the same method proposed by Sztaray and Baer,⁵ except that the discrete anodes are now replaced with virtual image regions, meaning that the position and area of these circular regions can be chosen *a posteriori*. This approach is illustrated in Fig. 3(a), where a close up of a photoelectron image of Ar integrated in the photon energy range 15.925–15.94 eV is shown. At this energy nearly all the electrons correspond to the $^2P_{1/2}$ threshold since the $^2P_{3/2}$ level would give 184 meV electrons which are strongly discriminated by the low repeller voltage.

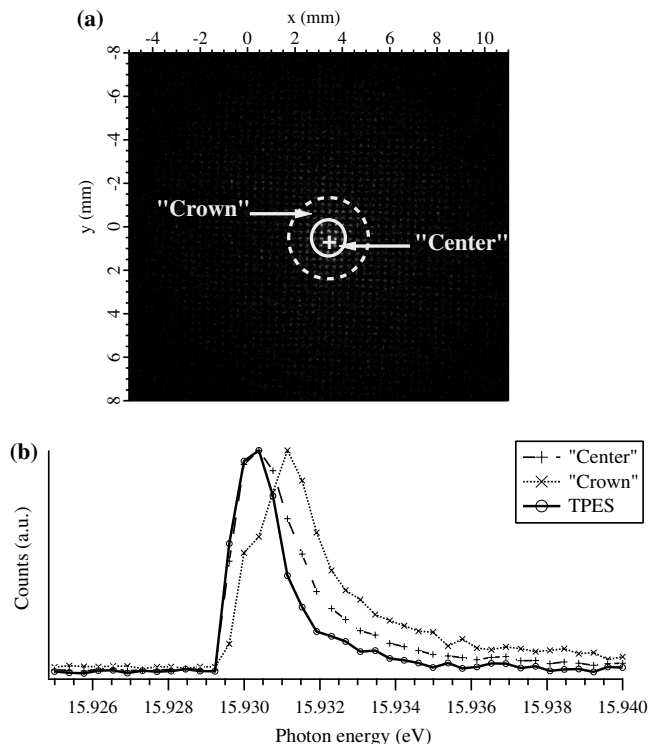


FIG. 3. Illustration of the method described in this work to select threshold electrons from the photoelectron image. (a) Complete photoelectron image of argon obtained in the 15.925–15.94 eV energy range using multibunch SR with a repeller of -25 V. The $+$ sign indicates the center of the image. The “center” and “crown” regions are delimited by the solid and dotted lines with, respectively, 1.8 and 4.6 mm external diameters. The PES corresponding to the photoelectrons located in the center and in the crown are shown in the bottom graph as dashed and dotted lines, respectively. Subtraction of the crown from the center after normalization with an appropriate factor (0.8 in this case) leads finally to the TPES represented by solid line.

The central region marked in Fig. 3(a) corresponds to a diameter of 1.8 mm over the total 40 mm diameter of the detector, while the outer ring or crown is fixed to the central region and has an external diameter of 4.6 mm. The signal obtained from the crown provides an evaluation of the hot electron contribution. Assuming a constant contribution of the hot electrons to the crown and center, a simple renormalization by the area of the two regions and a subtraction provides therefore a pure threshold photoelectron signal. However when the kinetic energy of the hot electrons is close to the radial position of the crown, as obtained from Eq. (1), the contribution of the energetic electrons to the crown and center is no longer constant and has to be taken into account by an empirical factor f . The subtraction then takes the shape

$$\text{TPES} = \frac{\text{Center}}{A_{\text{center}}} - f \frac{\text{Crown}}{A_{\text{crown}}}, \quad (2)$$

where A represents the area of either the central or the crown zones on the PSD. Since the factor f depends on the form of the TPES and on the angular distribution of the hot electrons,⁵ the normalization factor will vary for each studied system and with the photon energy for very large scans. In practice, an optimum factor can be automatically found as the highest value for which the baseline is positive. Experimentally this optimum factor varies between 0.5 and 0.8.

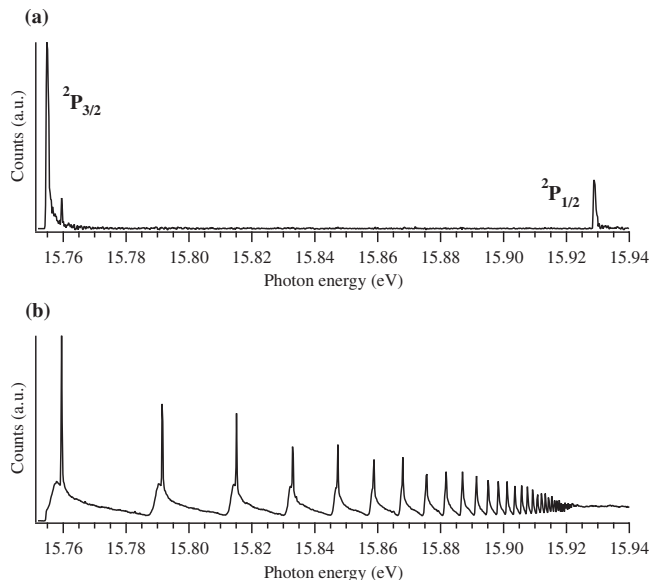


FIG. 4. (a) TPES of argon and (b) corresponding simultaneously recorded total ion yield spectrum in the 15.75–15.94 eV energy range obtained with a repeller of -5 V and a photon bandwidth of 0.28 meV. To obtain this spectrum, center and crown region diameters of 1.4 and 2.7 mm were used.

The TPES of the $2P_{1/2}$ Ar threshold obtained in the 15.925–15.94 eV energy region is given as an illustration of the subtraction method in Fig. 3(b). The center and crown raw spectra obtained by selecting the regions of Fig. 3(a) are plotted along with the subtracted result. The center spectrum shows a tail due to the hot electron contribution to the central region. To reduce this hot-electron tail, the signal corresponding to the crown region is subtracted with a correction factor of 0.8. The resulting TPES is then free of almost all hot electron contributions, as can be seen in Fig. 3(b).

In order to show the high energy resolution capability of the method as well as the long-term signal-to-noise ratio and stability, we present in Fig. 4 the TPES obtained for the two first ionization thresholds of argon in the 15.75–15.94 eV energy range with 0.2 meV steps and using a repeller voltage of 5 V and center and crown diameters of 1.4 and 2.7, mm respectively. The measured energy resolution (full width at half maximum) reached is of 0.8 meV for both thresholds. This spectrum was taken with the 2400 gr/mm monochromator grating and ~ 20 μm slits corresponding to a photon resolving power of $\sim 60\,000$. Each point was accumulated during 2.5 s. Note that this resolution of 0.8 meV is obtained in the full TPEPICO mode, i.e., by detecting in coincidence the TPE with the corresponding mass-selected ion.

The corresponding total ion yield spectrum recorded simultaneously shows the ns' and nd' Rydberg autoionizing series converging toward the $2P_{1/2}$ limit with slit-limited resolution (0.28 meV). These resonances decaying via autoionization and producing fast electrons are totally suppressed in the TPES spectrum, which only shows the two $3p^{-1}$ ionic states of Ar, except for a tiny contribution from the exceptionally intense $11s'$ Rydberg state around 15.76 eV. On the resonances, the total electron count rate exceeded 20 000 cps (counts per second), while count rates within the central and crown regions reached up to 200 and 500 cps, respectively. It should be noted that when performing TPES with a VMI

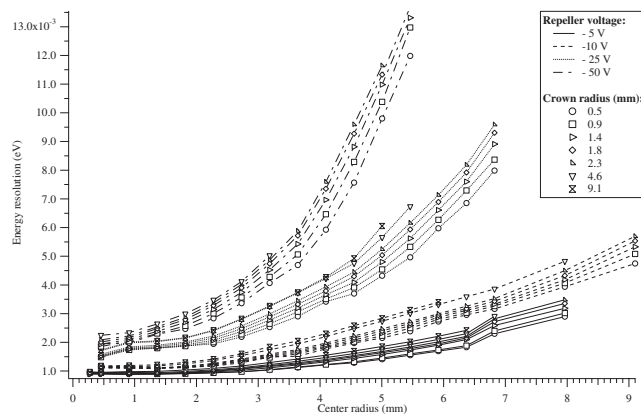


FIG. 5. Variation in the measured energy resolution (in eV) of the Ar $2P_{1/2}$ TPES signal (in the 15.93 eV energy region) as a function of the size of the center region diameter (in millimeters) for different voltages applied to the repeller electrode (-5 , -10 , -25 , and -50 V) and different sizes of the crown region diameter (from 0.9 to 18.2 mm).

spectrometer, attention has to be paid to detector saturation since threshold electrons arrive within a small area of the detector. At the moment of writing, the MCPs mounted on the detector have 32 μm pore separation and 1.5 mm thickness. Because each channel within the MCP has a dead time of a few tens of milliseconds⁴³ and, in the example shown in Fig. 4, the central region encircles only 50 channels, the maximum count rate in the center will be limited to a few thousands cps. However, we expect the dead time to decrease with the density of channels so that a future improvement in maximum count rate will be achieved by installing thinner MCPs with a shorter pore to pore distance and lower resistance.

The performance of the VMI spectrometer in the threshold mode is more generally characterized in Fig. 5, where the dependence of the energy resolution with the repeller voltage and the central and crown region size is described. As already discussed earlier, the resolution is improved for lower repeller voltages because the fast electrons are more efficiently dispersed. For instance, for a fixed size of center (4.6 mm) and crown (1.8 mm) diameters, the resolution degrades from 1.3 to 8.5 meV when increasing the repeller from 5 to 50 V. This result, however, disagrees with the theoretical predictions since the energy resolution should be proportional to the repeller. This can be explained by the importance of stray fields at very low repellers. From the curves, we can state that the resolution is indeed proportional to the repeller when its value is above 10 V. Repeller voltages under this value will begin to saturate the resolution.

Ray tracing simulations predict a dependence on R^2 for the threshold electron energy resolution and for a fixed crown region of the form

$$\Delta E = a + bR^2, \quad (3)$$

where a is an offset limiting the lowest possible resolution due to the finite size of the source and b depends linearly on the repeller voltage. The experimental curves plotted in Fig. 5 follow the theoretical trend although the absolute values differ slightly, as noted in Table I, where the theoretical values are written alongside the experimental results.

TABLE I. Electron energy resolution in the TPES/TPEPICO modes: experimental values along with the (bracketed) theoretical predictions for several repeller voltages and central region diameters. The numbers are given in meV for a fixed crown diameter of 3.6 mm and a normalization factor f of 0.5.

Repeller (V)	Central region diameter		
	0.9 mm	4.6 mm	9.1 mm
5	0.8(0.2)	1.0(0.4)	1.1(1.0)
10	1.1(0.2)	1.1(0.6)	1.5(1.7)
25	1.5(0.2)	2.0(1.1)	4.2(4.1)
50	2.0(0.3)	3.0(2.0)	9.0(7.9)

By looking at the table we can conclude that the agreement is worst for the small repeller values and central regions, which can be explained by penetrating and stray fields, mechanical defects producing electrostatic aberrations, or an interaction region larger than expected.

Due to its simplicity, the TPES method presented here can be applied straightforwardly to any VMI spectrometer with a PSD detector. The resolution has been improved with respect to the original experimental setup of Sztaray and Baer⁵ partly because the imaging capabilities allow a greater flexibility on the selection of the central and crown regions, which means that we can adjust the position and size to find the optimum subtraction. This is of critical importance when applying very low values on the repeller, where the center of the image can move due to stray fields or mechanical misalignments. Furthermore, by decreasing the size of the central area, it is possible to keep a reasonably high electron resolution while having high extraction fields, and therefore a high mass resolution (see Sec. IV). In this sense, the PSD provides a great versatility in the optimization of the compromise between electron energy resolution and mass resolution of the corresponding ion in the context of TPEPICO experiments. In addition, this flexibility allows for a given repeller voltage to tune the trade off between electron resolution and the signal level.

In comparison with the PFI-TPEPICO setup as developed at the Advanced Light Source,⁴ our system is able to reach a similar ultimate electron energy resolution, with a fully continuous and simple system, without the need for complex pulse shaping electronics necessary to optimize the PFI process and without the trouble of treating false coincidence in a pulsed regime. In addition, as already pointed out by Sztaray and Baer,⁵ the focusing optic TPE selection is compatible with the presence of high extraction fields which may be necessary for optimum mass resolution on the ion side (to the detriment of electron energy resolution), a compromise that cannot be found with the PFI-TPEPICO method in which the average extraction field is rather low to ensure a correct PFI process.

IV. PERFORMANCE OF THE WM-TOF

The performances of the WM spectrometer are already well described analytically.²² In our case, the light source dimension along the spectrometer's axis defines the uncertainty on the ion's creation dimension Δs around the point

source s_0 , where s_0 is the distance from the ionization source to the repeller plate. This dimension depends on the aperture of the monochromator's exit slit and typically varies between 100 and 300 μm . Assuming the largest aperture, the mass resolution obtained for ions with no initial kinetic energy under the space focusing condition $(d\text{TOF}/ds)_{s_0}=0$ is $M_{\Delta s}=2859$ amu.

For particles having an initial kinetic energy E_0 , including thermal energy, the mass resolution depends on the time it takes for an ion ejected opposite to the detector's direction to double back,

$$M_{\Delta E} \propto \left(\frac{1}{\sqrt{t_r}} \right),$$

$$t_r = \frac{4E_0 s_0}{qV_{\text{rep}}(1-\rho)}, \quad (4)$$

where $\rho = V_{\text{ext}}/V_{\text{rep}}$ and V_{ext} (V_{rep}) is the voltage applied to the extractor (repeller) electrode. The expression illustrates the natural compromise between the electron and mass resolutions when operating in coincidence mode with threshold electrons (see Sec. III).

The analytical expectations need to be compared to our actual design. Indeed, due to the gridless design of the extractor plate, the electric field is not homogeneous and varies along the spectrometer's axis, as well as on the plane perpendicular to this direction. Owing to the MB diameter at the ionization region, the cigar-shaped volume source presents the largest dimension along the SR direction. Ions created along this direction will be submitted to different focusing conditions, which will translate in an asymmetry on the TOF peak shape. Electrostatic simulations demonstrate that the electric field can decrease by a few percent along the SR axis, which causes a tail toward longer TOFs to appear. This effect is illustrated in Fig. 6, where a mass spectrum of Xe recorded for $V_{\text{rep}} = -100$ V is presented. The top graph shows the ion TOF obtained under VMI conditions while in the bottom one the extractor voltage has been lowered to diminish the lens effect at the ionization point. Clearly the asymmetric shape observed in Fig. 6(a) is related to the inhomogeneous electric field created by the gridless design.

Furthermore the electric field is globally increased in the direction of the spectrometer's axis due to the potential isocurves "leaking" through the gridless electrodes. Therefore, to compensate for this effect, the expected ratio between the first and second acceleration regions of the WM has to be increased by a factor of ~ 1.2 .

The mass resolution calculated by applying the WM expressions to the conditions stated in Fig. 6 is $M_R = 107$ amu. This value is derived assuming the velocity distribution found in a MB cooled at 40 K and represents the maximum mass for which we should resolve M_R and $M_R + 1$. By studying Fig. 6(a), we can conclude that the inhomogeneous field does not degrade significantly the mass resolution, even if the TOF peaks are distorted, since all the Xe isotopes around $m/z = 132$ are clearly separated from adjacent masses. We can also express the resolution in terms of mass or time

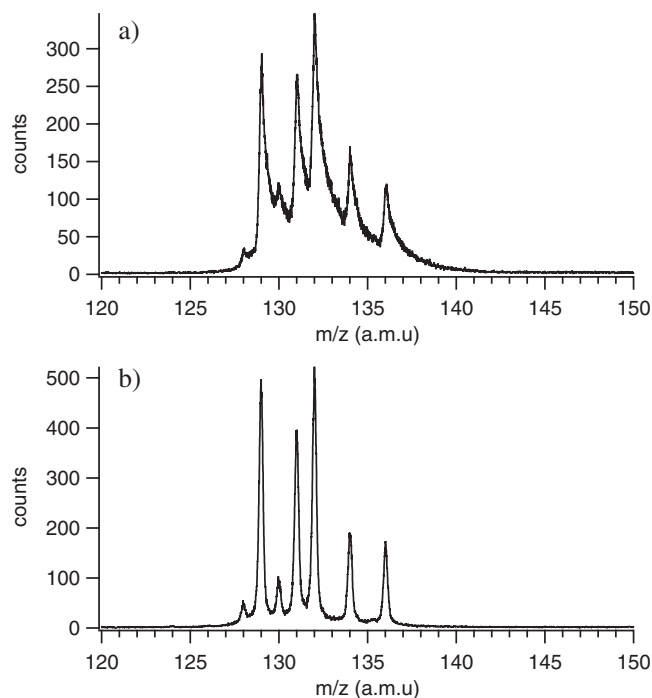


FIG. 6. Xe TOF recorded at 12.5 eV showing the effect of the inhomogeneous extraction field on the peak shapes. The repeller was set at 100 V and ion space focusing conditions were applied. (a) VMI focusing conditions ($\rho=0.714$). (b) Lower ratio ($\rho=0.5$) to decrease the lens effect.

resolving power, and for the case described in Fig. 6(a), under VMI conditions, we obtain $M/M_{\text{FWHM}}=t_M/2t_{\text{FWHM}}=265$ for the peak at 132 amu.

This example illustrates the ability of our spectrometer to reach satisfactory mass resolutions even for a relatively low repeller voltage, whereas, as seen in Sec. III, keeping an electron resolution of a few meV. The narrower transverse speed distribution obtained in the MB due to the cooling process contributes to increase further the mass separation of the parent ions. If one is only interested in purely mass spectroscopic studies without the need for selecting the electron's energy, the ratio ρ could be diminished to eliminate the asymmetric TOF shape and increase the mass resolution.

Another important aspect of the WM-TOF, which also imposes a lower limit on V_{rep} in coincidence mode, is the ion transmission. Since the MB is propagating perpendicular to the spectrometer's axis, the ions need to be accelerated enough perpendicularly to their initial momentum to cross through the electrodes and reach the PSD. Geometrical constraints on the SAPHIRS chamber prevented us from increasing the electrode internal radii so that, even with the addition of deflectors, we are limited to the detection of light masses at low repeller voltages. With our current geometry the lower limit for the ion masses to achieve 100% collection of the ions can be expressed, via the basic application of dynamics laws, as a function of the repeller using the expression

$$(m/z)_{\text{limit}} = 5.41 \times 10^6 \frac{V_{\text{rep}}}{v_{\text{jet}}^2}, \quad (5)$$

where the mass is given in amu, the repeller in volts, and v_{jet} is the MB velocity in m/sec. For instance, lowering the re-

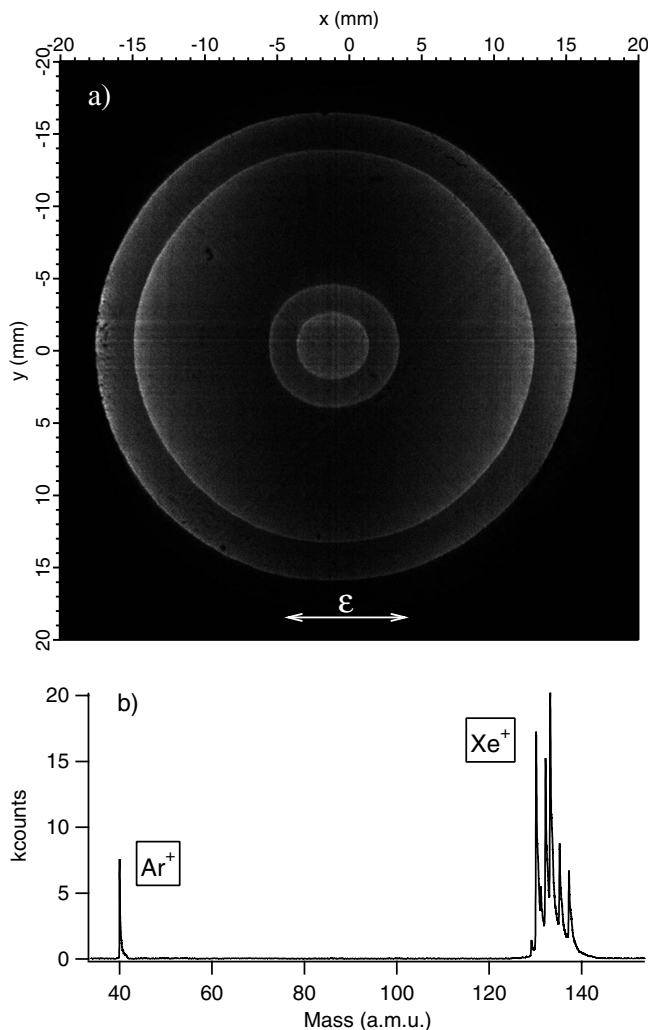


FIG. 7. (a) Photoelectron image of an Ar/Xe mixture taken at $h\nu=16$ eV and $V_{\text{rep}}=1500$ V. The electric vector of the light ε is shown in the image. The acquisition count rate was 13 and 7.1 kHz for the electrons and ions, respectively. The image was accumulated in less than 10 min. (b) TOF spectrum taken in coincidence with the electron image.

pellor voltage to -10 V will limit our detection to masses under 27 amu when using a supersonic Ar seeded beam cooled at 40 K due to the high speed (~ 1400 m/s) along the MB direction. The use of -50 V on the repeller would raise the mass limit up to 135 amu, which is enough for most of our applications, and corresponds to a typical electron energy resolution of 2 meV, very satisfactory in the case of large organic molecules.

V. COINCIDENCE PERFORMANCES

A. The AR-PEPICO mode of operation

There are two main approaches when performing coincidences with DELICIOUS II. The first one consists of recording photoelectron images of a given ion mass (PEPICO). This is illustrated in Fig. 7 where the photoelectron image shown corresponds to the photoionization of a mixture of Ar and Xe at a photon energy of 16.0 eV. This energy is above the first $3p^{-1}$ and $5p^{-1}$ ionization potentials of Ar and Xe, respectively. Four rings can be discerned, two for each atom corresponding to the $^2P_{3/2}$ and $^2P_{3/2}$ states of the ion. Figure

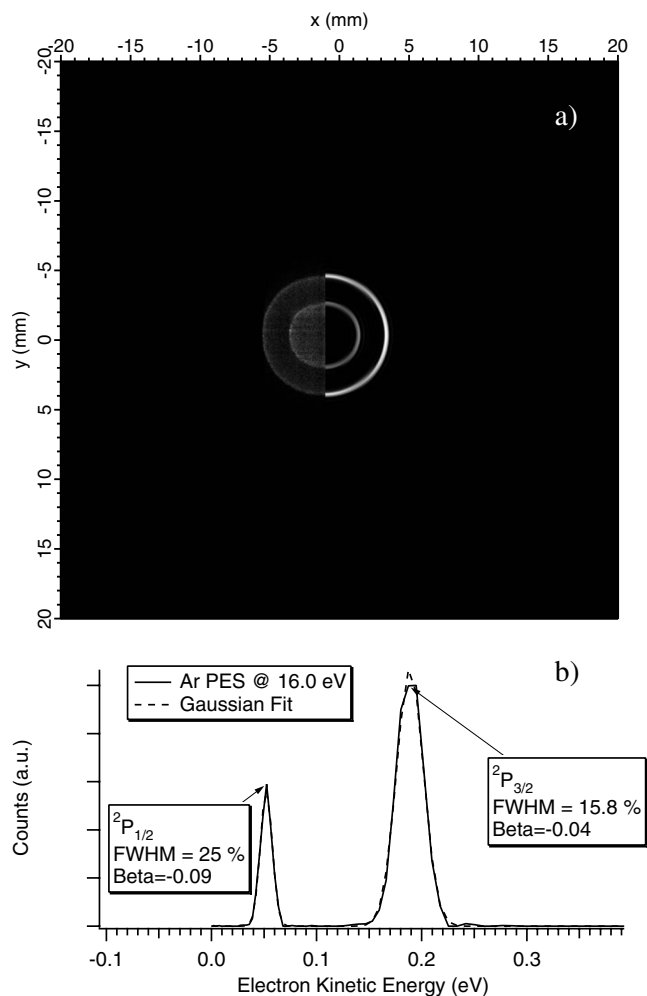


FIG. 8. (a) Ar photoelectron image obtained by taking all the electrons in coincidence with the Ar mass peak. The left side of the image represents the raw data while the right side corresponds to the pBasex reconstructed image. (b) Ar photoelectron spectrum showing the two spin orbit states. The text boxes describe the energy resolution and the β angular parameter for each ionized orbital.

7(b) also shows the ion TOF obtained in coincidence with the electron image, where two groups of peaks corresponding to the Ar and Xe masses can be observed, including the different Xe isotopes. The electron image and the ion TOF have been acquired during less than 10 min with a respective counting rate of 13 and 7.1 kHz. Out of the 13 000 events per second read by the TDC, only 22% was accepted as true coincidences while the rest was rejected due to electron position or ion missing from the event. By selecting the ionization events corresponding to a given mass range, we can obtain photoelectron images for the individual species present in the MB, as demonstrated in Figs. 8 and 9 for the Ar and Xe peaks, respectively. The photoelectron images are subsequently treated by applying the pBasex algorithm⁴⁴ to extract a slice of the original 3D sphere. After the image inversion, the generation of the PES and angular parameters is straightforward. As it can be seen in Figs. 8(b) and 9(b), the ion filtering of the electron images leads to clean PES without any background coming from scattered light or from residual gases.

As stated in our previous work,¹³ the relative kinetic

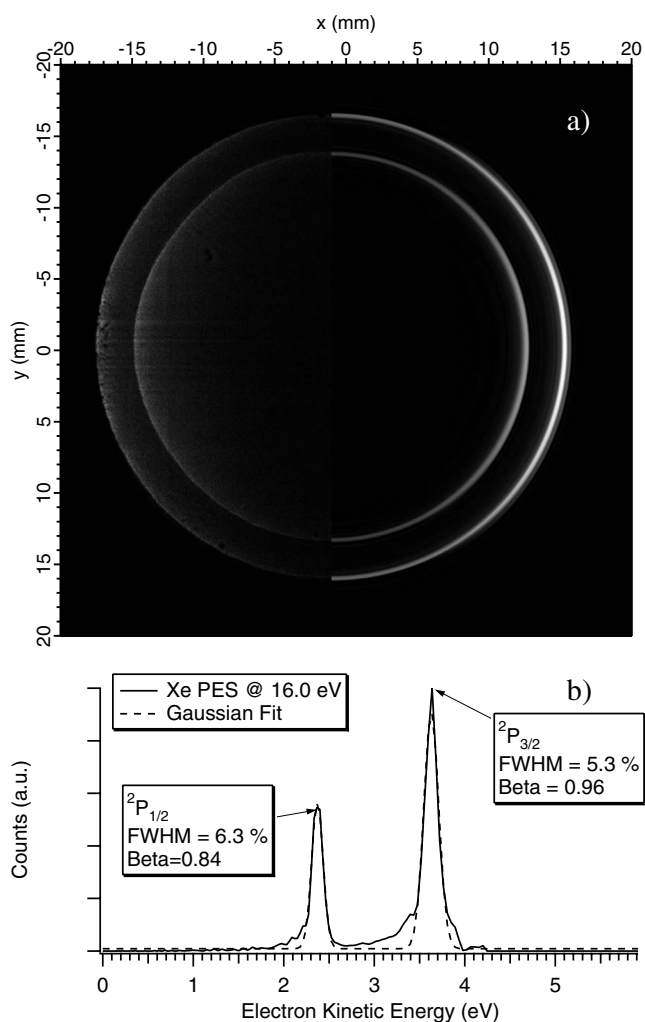


FIG. 9. (a) Xe photoelectron image obtained by taking all the electrons in coincidence with the Xe mass peak, all isotopes included. The left side of the image represents the raw data while the right side corresponds to the pBasex reconstructed image. (b) Xe photoelectron spectrum showing the two spin orbit states. The text boxes describe the energy resolution and the β angular parameter for each ionized orbital. The radial dependence of the kinetic energy resolution dramatically improves it with respect to the Ar PES in Fig. 8(b).

energy resolution depends on the ratio between initial kinetic energy and the repeller voltage. For this particular example, the resolution varies between 25% at the lowest ratio (Ar $^2P_{1/2}$) and 5.3% at the highest ratio (Xe $^2P_{3/2}$). This figure could probably be even lowered (<5%) by slightly lowering the repeller voltage so that the corresponding outer ring would approach the edge of the PSD. The energy resolution has been perceptively improved with respect to the previous publication¹³ probably due to the smaller beam size provided by the DESIRS beamline. The resolution achieved with DELICIOUS II shows its clear advantage over imaging detectors whose electron energy resolution depends on the TOF, and which is typically limited to few tens of percent as soon as the kinetic energy of the electron is above 1 eV or so. Although recent advances in timing electronics have allowed 3D imaging analyzers to attain resolutions of a few percent,²⁹ they are still limited to relatively slow electrons and need to pulse the extraction field to elongate the electron's TOF. In addition they require a pulsed light source with a very short

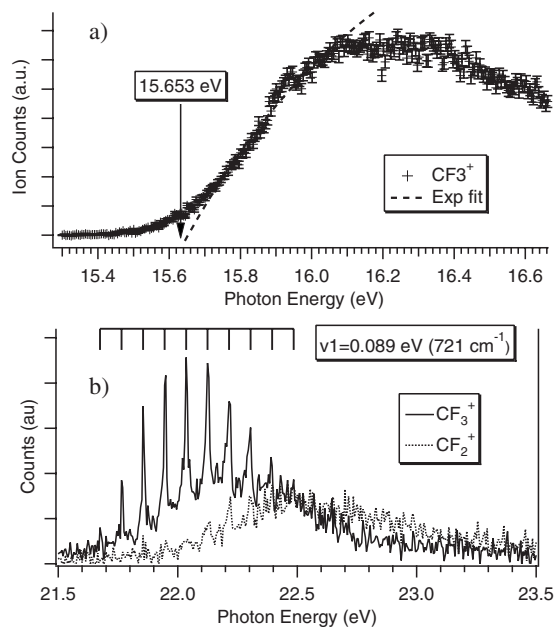


FIG. 10. CF_4 TPEPICO spectra recorded with a photon resolution set to 15 meV, while the threshold electrons were selected with 15 meV resolution by applying a repeller voltage of 50 V, i.e., an overall resolution of 21 meV. (a) CF_4 TPEPICO showing the photoionization to the ionic ground state \tilde{X} . The markers correspond to the experimental data while the dashed line represents an exponential fit. (b) TPEPICO curves for the \tilde{C} ionic state showing the two fragmentation channels CF_3^+ (solid line) and CF_2^+ (pointed line). The breathing vibrational progression is also depicted at the top of the graph. For CF_2^+ , the threshold electron resolution has been degraded to 20 meV (25 meV overall resolution) to improve the data quality.

pulse duration which cannot be achieved on third generation SR sources, where pulse durations even in the time-structure mode are in general of the order of 40–80 ps.

For one-photon direct ionization with linearly polarized light, the angular distribution of electrons ejected from a randomly oriented sample is fully characterized in the laboratory frame by the well-known β parameter. The measured angular parameters for the four orbitals probed [Figs. 8(b) and 9(b)] are in good agreement with previous experimental results on rare gases,⁴⁵ showing that DELICIOUS II is well suited for AR-PES on mass-selected samples.

B. The TPEPICO mode of operation

The second approach consists of performing coincidences with threshold electrons to select the ion's internal state. Scanning the photon energy while fixing the kinetic energy of the electron to zero permits the study of the energetics and fragmentation pathways as a function of the ion's internal energy.

As an example, we have recorded TPEPICO spectra of the CF_4 molecule over a range of energies going from the first IP up to 23.5 eV. We chose this system because it has been already studied extensively by different groups^{46–48} and therefore can be used in the context of an instrumental paper as a performance benchmark. The molecule has the particularity to fragment directly in all of its ionic states, leading mostly to the formation of the CF_3^+ ion. Thus, the CF_4^+ ion is never observed. The first threshold onset corresponding to the ground ionic state is shown in Fig. 10(a). The data were

recorded on a supersonically cooled beam of 99.9% pure CF_4 obtained from Aldrich using the 200 gr/mm monochromator grating of DESIRS with the slits set to obtain a photon resolution of 15 meV. The threshold electrons were selected with a resolution of 15 meV leading to an overall 21 meV of the TPEPICO spectra. By fitting an exponential curve on the experimental data we can estimate the first IP to be $\text{IP}(\tilde{X}) = 15.65 \pm 0.01$ eV, although this measure is unlikely to represent the adiabatic value. Velocity map ion imaging experiments looking at the dissociation of CF_4^+ have shown a Jahn–Teller effect which breaks the symmetry of the images, pointing to a change in geometry that would disfavor an adiabatic transition.⁴⁸ Assuming a perfect MB expansion where the internal energy of CF_4 can be neglected, we can estimate the adiabatic IP as the first point that deviates from the background by a value larger than its error bar to obtain $\text{IP}_{\text{ad}}(\tilde{X}) = 15.45 \pm 0.02$ eV. This value is 0.1 eV higher than the one previously published by Creasey *et al.*⁴⁶ and in accordance with He I experiments (≥ 15.35).⁴⁹ This discrepancy cannot be explained solely by the temperature difference between our MB and their effusive jet. However it should be noted that no error bars were included by these groups, while ours are taking into account data statistics and the absolute precision of the 200 gr/mm monochromator's grating, which is estimated at ~ 5 meV (note that the other gratings of the monochromator provide an absolute accuracy of 1 meV). The ~ 0.2 eV slow onset in the TPEPICO curve from the estimated IP_{ad} until reaching the expected exponential behavior might signify that vertical, more energetic transitions are more probable.

Also of interest is the \tilde{C} ionic state illustrated in Fig. 10(b). The TPEPICO spectrum of this state, recorded with the same 21 meV overall resolution, has already been obtained by Creasey *et al.*⁴⁶ but with a significantly lower resolution (80 meV). We measure an adiabatic ionization potential of $\text{IP}(\tilde{C}) = 21.68 \pm 0.01$ eV from the CF_3^+ fragment curve, in good agreement with the previously published value⁴⁶ of 21.67 ± 0.03 eV. Owing to our high resolution, we can very clearly observe the long vibrational progression of the ν_1 symmetric stretching mode, peaking at $\nu_1=4$, with a frequency of 721 ± 6 cm^{-1} (0.0895 ± 0.0008 eV), while a value of 702 ± 40 cm^{-1} has been published by Creasey *et al.*⁴⁶ Note that our value is in very close agreement with the value of 729 ± 1 cm^{-1} obtained by high resolution $\tilde{D} - \tilde{C}$ emission spectrum.⁵⁰

In addition to the production of CF_3^+ , a competing fragmentation pathway is made available in this ionic state, leading to the formation of the CF_2^+ fragment. Since the CF_2^+ signal is significantly weaker than that of CF_3^+ , we have chosen to degrade the electron resolution to 20 meV in order to increase the signal-to-noise ratio, leading to an overall resolution of 25 meV. In these conditions, we can determine the appearance potential of the CF_2^+ fragment, which coincides with the $n=2$ vibrational band, i.e., $\text{AP}(\text{CF}_2^+) = 21.86 \pm 0.02$ eV. This difference of 0.18 eV between the onset of the CF_3^+ and CF_2^+ pathways has already been discussed by Creasey *et al.*⁴⁶ and indicates an energy dependence of the two competing channels on the \tilde{C} ionic state

potential energy surface, CF_3^+ being produced by dissociation in the \tilde{X} and \tilde{A} states after radiative decay from the \tilde{C} state, while CF_2^+ would be produced by direct fragmentation from the \tilde{C} state.

C. Considerations on false coincidences

Up to now we have not introduced the treatment of false coincidences. Contrary to the VMI single mode where the count rate is only restricted to the dead time of the detector (6.5 MHz), the coincidence mode needs to operate with lower count rates in order to limit false coincidences. In fact, the limitation arises from the timing window (see Sec. II) opened by the arrival of the electrons, during which only the ion arrival is recorded and no further electron signals are allowed. Thus, to minimize false coincidences, the electron counting rate is kept under the window's maximum frequency (1/period). For instance in the Ar+Xe example, the maximum TOF allowed is 8 μ s, limiting the maximum count rate to 125 kHz. The actual recording rate for this image was 13 kHz due to data flow limitations on the TDC. This ratio of ~ 10 between the actual counting rate and the maximum possible counting rate insures a very low level of false coincidences, as it can be seen on the TOF spectrum of Fig. 7(b) on which no background can be seen. Note that for heavier masses or lower repeller voltages where the maximum allowed TOF will be longer, the count rate will have to be decreased.

The occurrence of false coincidences has been minimized in the present design due to the 4π collection on both the electron and ion spectrometers, which is not the case when one uses electrostatic analyzers, for instance. The only discrimination here stems from the presence of additional grids on the ion side, which reduces the ion count by a factor of ~ 2 with respect to the electrons.

Even in the coincidence mode, DELICIOUS II operates continuously without needing to pulse the extraction plates. This presents a major advantage when dealing with false coincidences because they will be spread evenly along the TOF spectrum giving a flat background. Subtraction of this background is then straightforward, as opposed to a pulsed mode where complicated treatment schemes have to be devised.²³ Contrary to other spectrometers which need the pulsed mode to ensure a good electron time resolution,^{29,30} we would use such a pulsed mode only when doing very high resolution TPEPICO studies on heavy molecules.

VI. CONCLUSION

We have presented a coincidence spectrometer capable of recording mass-selected velocity mapped images of photoelectrons maintaining an excellent compromise between fast and threshold electron energy resolution and ion mass resolution. The apparatus is extremely versatile, capable of analyzing and detecting at high counting rates electrons with kinetic energies in a very large range from 0 to 17 eV, with sub-meV resolution from threshold electrons and close to 5% for fast electrons. This large versatility meets the needs of the broad scientific program we wish to cover with the DESIRS beamline at SOLEIL. The threshold electron resolution is

comparable to that obtained using pulsed field ionization coincidence (PFI-PEPICO) techniques⁴ but without the need for complicated pulsed shapes or the synchrotron's time structure.

On the ion side we can reach mass resolutions of 130 amu even for very low repeller voltages. This mass resolution ameliorates with the square root of the repeller for experiments demanding higher resolutions so that MS studies where the electron energy resolution is not an important issue could be performed with mass resolutions above 1000 amu. However, due to the asymmetric peak shapes produced by the VMI focusing conditions, the extraction of KER information by modeling the fragment TOF shape is not possible in combination with high threshold energy resolution.

The spectrometer is well adapted to SR and benefits from its time structure, low density photon pulse so that at most one event is produced per pulse, which limits false coincidences while keeping a very high repetition rate ensuring high data statistics.

Furthermore, DELICIOUS II does not employ any electron TOF measurement and, hence, is operated in a pure continuous mode without the dependence that other spectrometers may have on the time structure of the light source. This point is especially important for synchrotron facilities where the few-bunch mode of operation is less and less available due to the associated severe reduction in flux. The continuous mode also facilitates dramatically the treatment of false coincidences. The position sensitive detection system has been chosen by its very low dead time to allow electron/ion correlation in an event per event basis.

DELICIOUS clearly surpasses the former TPEPICO (Ref. 34) spectrometer of SAPHIRS by its versatility (possibility to also perform AR-PEPICO), its electron resolution, improved by a factor of 5–10, and its ability to work in a pure continuous mode in the multibunch mode of operation.

Finally, as in the design proposed by Rolles *et al.*,²⁰ the spectrometer can also be employed for mass-selected ion VMI. Indeed, by inverting the electrodes' polarity and detecting the electrons with the WM-TOF, ion images can be recorded along with their TOF, on the VMI side, in a pure continuous mode.

Future improvements to DELICIOUS II are already scheduled. Regarding the electronics, a new TDC will replace the CTNM4 TDC so that the counting rate will be only limited by the detector's dead time, which we plan to also improve with shorter pore to pore distances. In addition, we plan to add a diverging lens on the VMI spectrometer, as the one commonly used in photoionization microscopy imaging experiments.⁵¹ Such a lens would further help to discriminate fast electrons so that the TPES resolution would be nearly photon bandwidth limited. In the TPEPICO mode of operation, this improved electron resolution would also allow us to apply higher voltages on the extraction plates, removing the need for compromising between mass resolution and geometrical ion transmission and electron resolution.

ACKNOWLEDGMENTS

The authors would like to acknowledge the important contribution of B. Pilette for the mechanical conception and

assembling of DELICIOUS II. We are also indebted to the general technical staff of SOLEIL for running the facility.

- ¹ *High Resolution Laser Photoionization and Photoelectron Studies*, edited by I. Powis, T. Baer, and C.-Y. Ng (Wiley, New York, 1995); *VUV and Soft X-Ray Photoionization*, edited by U. Becker and D. A. Shirley (Plenum, New York, 1996).
- ² K. Ueda, *J. Electron Spectrosc. Relat. Phenom.* **141**, 73 (2004); R. E. Continetti, *Annu. Rev. Phys. Chem.* **52**, 165 (2001).
- ³ T. Baer, J. Booze, and K. M. Weitzel, in *Vacuum Ultraviolet Photoionization and Photodissociation of Molecules and Clusters*, edited by C. Y. Ng (World Scientific, Singapore, 1991), p. 259.
- ⁴ G. K. Jarvis, K. M. Weitzel, M. Malow, T. Baer, Y. Song, and C. Y. Ng, *Rev. Sci. Instrum.* **70**, 3892 (1999).
- ⁵ B. Sztaray and T. Baer, *Rev. Sci. Instrum.* **74**, 3763 (2003).
- ⁶ G. A. Garcia, P. M. Guyon, and I. Powis, *J. Phys. Chem. A* **105**, 8296 (2001).
- ⁷ C. Y. Ng, *J. Phys. Chem. A* **106**, 5953 (2002); C. Alcaraz, C. Nicolas, R. Thissen, J. Zabka, and O. Dutuit, *ibid.* **108**, 9998 (2004).
- ⁸ D. Dowek, M. Lebech, J. C. Houver, and R. R. Lucchese, *J. Electron Spectrosc. Relat. Phenom.* **141**, 211 (2004).
- ⁹ D. W. Chandler and P. L. Houston, *J. Chem. Phys.* **87**, 1445 (1987).
- ¹⁰ A. G. Suits and R. E. Continetti, *Imaging in Chemical Dynamics* (American Chemical Society, Washington, DC, 2000).
- ¹¹ A. T. J. B. Eppink and D. H. Parker, *Rev. Sci. Instrum.* **68**, 3477 (1997).
- ¹² D. S. Peterka, M. Ahmed, C. Y. Ng, and A. G. Suits, *Chem. Phys. Lett.* **312**, 108 (1999); Y. Hikosaka and E. Shigemasa, *J. Electron Spectrosc. Relat. Phenom.* **148**, 5 (2005).
- ¹³ G. A. Garcia, L. Nahon, C. J. Harding, E. A. Mikajlo, and I. Powis, *Rev. Sci. Instrum.* **76**, 053302 (2005).
- ¹⁴ Z. D. Pesic, D. Rolles, M. Perri, R. C. Bilodeau, G. D. Ackerman, B. S. Rude, A. L. D. Kilcoyne, J. D. Bozek, and N. Berrah, *J. Electron Spectrosc. Relat. Phenom.* **155**, 155 (2007).
- ¹⁵ K. Ueda and J. H. D. Eland, *J. Phys. B* **38**, S839 (2005).
- ¹⁶ P. Downie and I. Powis, *Phys. Rev. Lett.* **82**, 2864 (1999); J. A. Davies, R. E. Continetti, D. W. Chandler, and C. C. Hayden, *ibid.* **84**, 5983 (2000); A. Lafosse, M. Lebech, J. C. Brenot, P. M. Guyon, O. Jagutzki, L. Spielberger, M. Vervloet, J. C. Houver, and D. Dowek, *ibid.* **84**, 5987 (2000).
- ¹⁷ M. Takahashi, J. P. Cave, and J. H. D. Eland, *Rev. Sci. Instrum.* **71**, 1337 (2000).
- ¹⁸ For general information on the beamline's performance visit <http://www.synchrotron-soleil.fr/portal/page/portal/Recherche/LignesLumiere/DESIRS>.
- ¹⁹ M. Richard-Viard, O. Atabek, O. Dutuit, and P. M. Guyon, *J. Chem. Phys.* **93**, 8881 (1990).
- ²⁰ D. Rolles, Z. D. Pesic, M. Perri, R. C. Bilodeau, G. D. Ackerman, B. S. Rude, A. L. D. Kilcoyne, J. D. Bozek, and N. Berrah, *Nucl. Instrum. Methods Phys. Res. B* **261**, 170 (2007).
- ²¹ G. Prumper, H. Fukuzawa, T. Lischke, and K. Ueda, *Rev. Sci. Instrum.* **78**, 083104 (2007).
- ²² W. C. Wiley and I. H. Maclaren, *Rev. Sci. Instrum.* **26**, 1150 (1955).
- ²³ G. Prumper and K. Ueda, *Nucl. Instrum. Methods Phys. Res. A* **574**, 350 (2007).
- ²⁴ L. Nahon, G. A. Garcia, C. J. Harding, E. A. Mikajlo, and I. Powis, *J. Chem. Phys.* **125**, 114309 (2006).
- ²⁵ G. Garcia, L. Nahon, C. J. Harding, and I. Powis, *Phys. Chem. Chem. Phys.* **10**, 1628 (2008); I. Powis, C. J. Harding, G. Garcia, and L. Nahon, *ChemPhysChem* **9**, 475 (2008).
- ²⁶ T. Schüßler, H. J. Deyerl, S. Dümmler, I. Fischer, C. Alcaraz, and M. Elhanine, *J. Chem. Phys.* **118**, 9077 (2003).
- ²⁷ A. M. Schulenburg, C. Alcaraz, G. Grassi, and F. Merkt, *J. Chem. Phys.* **125**, 104310 (2006).
- ²⁸ M. Lebech, J. C. Houver, A. Lafosse, D. Dowek, C. Alcaraz, L. Nahon, and R. R. Lucchese, *J. Chem. Phys.* **118**, 9653 (2003); A. M. Rijs, M. H. M. Janssen, E. T. H. Chrysostom, and C. C. Hayden, *Phys. Rev. Lett.* **92**, 123002 (2004); J. Ullrich, R. Moshhammer, A. Dorn, R. Dorn, L. P. H. Schmidt, and H. Schmitt-Bocking, *Rep. Prog. Phys.* **66**, 1463 (2003).
- ²⁹ A. Vredenburg, W. G. Roeterdink, and M. H. M. Janssen, *Rev. Sci. Instrum.* **79**, 063108 (2008).
- ³⁰ M. Lebech, J. C. Houver, and D. Dowek, *Rev. Sci. Instrum.* **73**, 1866 (2002).
- ³¹ *Imaging in Molecular Dynamics*, edited by B. J. Whitaker (Cambridge University Press, Cambridge, England, 2003).
- ³² D. Ceolin, G. Chaplier, M. Lemonnier, G. A. Garcia, C. Miron, L. Nahon, M. Simon, N. Leclercq, and P. Morin, *Rev. Sci. Instrum.* **76**, 043302 (2005).
- ³³ M. H. Kim, B. D. Leskiw, L. Shen, and A. G. Suits, *Int. J. Mass. Spectrom.* **252**, 73 (2006); B. D. Leskiw, M. H. Kim, G. E. Hall, and A. G. Suits, *Rev. Sci. Instrum.* **76**, 104101 (2005).
- ³⁴ M. Richard-Viard, A. Delboulbe, and M. Vervloet, *Chem. Phys.* **209**, 159 (1996).
- ³⁵ O. Marcouille, P. Brunelle, O. Chubar, F. Marteau, M. Massal, L. Nahon, K. Tavakoli, J. Veteran, and J. M. Filhol, in *Synchrotron Radiation Instrumentation, Pts 1 and 2*, edited by J. Y. Choi and S. Rah (AIP, New York, 2007), Vol. 879, p. 311.
- ³⁶ L. Nahon, C. Alcaraz, J. L. Marlats, B. Lagarde, F. Polack, R. Thissen, D. Lepere, and K. Ito, *Rev. Sci. Instrum.* **72**, 1320 (2001).
- ³⁷ B. Mercier, M. Compin, C. Prevost, G. Bellec, R. Thissen, O. Dutuit, and L. Nahon, *J. Vac. Sci. Technol. A* **18**, 2533 (2000).
- ³⁸ T. Baer, P.-M. Guyon, I. Nenner, A. Tabche-Fouhaille, R. Botter, L. F. A. Ferreira, and T. R. Govers, *J. Chem. Phys.* **70**, 1585 (1979).
- ³⁹ R. I. Hall, L. Avaldi, G. Dawber, M. Zubek, K. Ellis, and G. C. King, *J. Phys. B* **24**, 115 (1991).
- ⁴⁰ C. W. Hsu, M. Evans, C. Y. Ng, and P. Heimann, *Rev. Sci. Instrum.* **68**, 1694 (1997).
- ⁴¹ R. I. Hall, A. McConkey, K. Ellis, G. Dawber, L. Avaldi, M. A. Macdonald, and G. C. King, *Meas. Sci. Technol.* **3**, 316 (1992).
- ⁴² G. K. Jarvis, Y. Song, and C. Y. Ng, *Rev. Sci. Instrum.* **70**, 2615 (1999).
- ⁴³ J. L. Wiza, *Nucl. Instrum. Methods* **162**, 587 (1979).
- ⁴⁴ G. A. Garcia, L. Nahon, and I. Powis, *Rev. Sci. Instrum.* **75**, 4989 (2004).
- ⁴⁵ D. M. P. Holland, A. C. Parr, D. L. Ederer, J. L. Dehmer, and J. B. West, *Nucl. Instrum. Methods Phys. Res.* **195**, 331 (1982).
- ⁴⁶ J. C. Creasey, H. M. Jones, D. M. Smith, R. P. Tuckett, P. A. Hatherly, K. Codling, and I. Powis, *Chem. Phys.* **174**, 441 (1993).
- ⁴⁷ T. Kinugawa, Y. Hikosaka, A. M. Hodgekins, and J. H. D. Eland, *J. Mass Spectrom.* **37**, 854 (2002).
- ⁴⁸ Y. Hikosaka and E. Shigemasa, *J. Electron Spectrosc. Relat. Phenom.* **152**, 29 (2006).
- ⁴⁹ C. R. Brundle, M. B. Robin, and H. Basch, *J. Chem. Phys.* **53**, 2196 (1970).
- ⁵⁰ J. F. M. Aarts, S. M. Mason, and R. P. Tuckett, *Mol. Phys.* **60**, 761 (1987).
- ⁵¹ H. L. Offerhaus, C. Nicole, F. Lepine, C. Bordas, F. Rosca-Pruna, and M. J. J. Vrakking, *Rev. Sci. Instrum.* **72**, 3245 (2001).